


# Strong exciton-localized plasmon coupling in a-Ge<sub>24</sub>Se<sub>76</sub>/AuNP heterostructure

Cite as: APL Mater. 4, 106105 (2016); <https://doi.org/10.1063/1.4964365>

Submitted: 19 August 2016 . Accepted: 23 September 2016 . Published Online: 07 October 2016

Rituraj Sharma, Pritam Khan, J. Aneesh, K. S. Sangunni, I. Csarnovics, S. Kokenyesi, H. Jain , and K. V. Adarsh



View Online



Export Citation



CrossMark

## ARTICLES YOU MAY BE INTERESTED IN

[Strong coupling in molecular exciton-plasmon Au nanorod array systems](#)

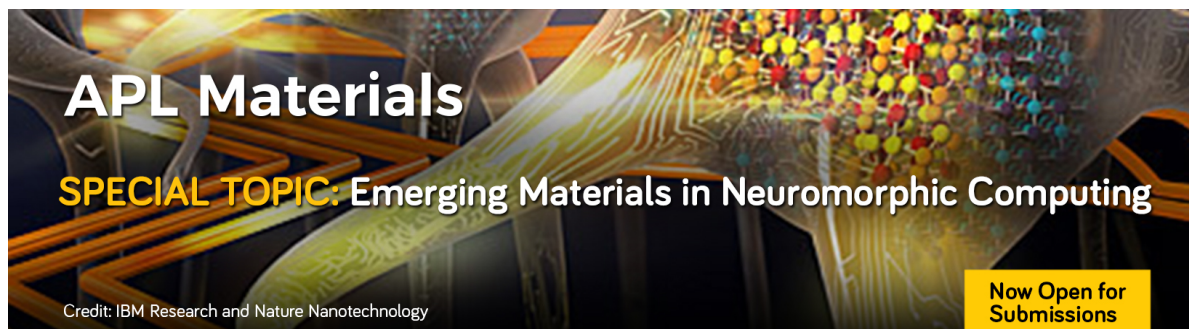
Applied Physics Letters **108**, 053102 (2016); <https://doi.org/10.1063/1.4941078>

[Light induced diffusion driven self assembly of Ag nanoparticles in a-Se/Ag bi-layer thin film with ultrafast optical response](#)

Applied Physics Letters **102**, 213110 (2013); <https://doi.org/10.1063/1.4807934>

[Pathway to oxide photovoltaics via band-structure engineering of SnO](#)

APL Materials **4**, 106103 (2016); <https://doi.org/10.1063/1.4963661>



## Strong exciton-localized plasmon coupling in a-Ge<sub>24</sub>Se<sub>76</sub>/AuNP heterostructure

Rituraj Sharma,<sup>1</sup> Pritam Khan,<sup>1</sup> J. Aneesh,<sup>1</sup> K. S. Sangunni,<sup>2</sup> I. Csarnovics,<sup>3</sup> S. Kokenyesi,<sup>3</sup> H. Jain,<sup>4</sup> and K. V. Adarsh<sup>1,a</sup>

<sup>1</sup>Department of Physics, Indian Institute of Science Education and Research, Bhopal 462066, India

<sup>2</sup>Department of Physics, Indian Institute of Science, Bangalore, India

<sup>3</sup>Institute of Physics, University of Debrecen, Debrecen, Hungary

<sup>4</sup>Department of Materials Science and Engineering, Lehigh University, Bethlehem, Pennsylvania 18015, USA

(Received 19 August 2016; accepted 23 September 2016; published online 7 October 2016)

Metal nanoparticle-semiconductor interfaces are sites of complex light-matter interactions, in particular, the exciton-plasmon coupling which plays a key role in the optical response of such heterostructures. There exists a pathway of photoinduced charge transfer from the semiconductor to the metal, which can be used to controllably vary the driving forces at the interface that leads to tunable optoelectronic properties. In this letter, we report the observation of a dramatic suppression of plasmonic as well as excitonic absorption in a-Ge<sub>24</sub>Se<sub>76</sub>/gold nanoparticle heterostructures by trapped charges. Suppression of the excitonic absorption is strongly correlated with the plasmon wavelength. © 2016 Author(s). All article content, except where otherwise noted, is licensed under a Creative Commons Attribution (CC BY) license (<http://creativecommons.org/licenses/by/4.0/>). [<http://dx.doi.org/10.1063/1.4964365>]

Exciton-plasmon coupling in a semiconductor/metallic hybrid structure can generate promising opportunities for new optical functionalities that are feasible with neither of the individual components of coupled states.<sup>1,2</sup> Although the coupling between the two quasi-particles, viz., plasmons and excitons are not yet fully understood, it is accepted that the surface plasmons in metal nanoparticles can trap and guide light at the nanoscale over broad spectral ranges.<sup>3</sup> This coupling depends on the characteristics of both the exciton related to the semiconductor and the plasmon related to metallic component in the hybrid. Over the last decade, a wide variety of exciton-plasmon interactions were studied with different kinds of materials and configurations like metal-core/semiconductor-shell heterostructures and metal-tipped semiconductor nanocrystals.<sup>4-6</sup> These studies have revealed light-matter interactions varying from weak to strong coupling regimes. In weak coupling, the wave function of the excitonic-plasmonic states is slightly modified such that the resultant optical properties are additive, i.e., the contributions from each layer are nearly independent and are simply added together with minor modifications. A typical example of such coupling is the fivefold enhancement of fluorescence in single CdSe(ZnS) core-shell nanocrystal quantum dots by plasmon interactions from a gold film.<sup>7</sup> On the other hand, in the strong coupling regime, the potential barrier at the interface is small, which allows inter-domain charge transfer across the layers.<sup>8,9</sup> Consequently, the electronic states at the interface become mixed and can result in new functionalities. For example, Lidzey *et al.* have reported polariton branches separated by Rabi splitting energy of 160 meV in an organic semiconductor inserted in the optical microcavity.<sup>9</sup> Furthermore, active inter-domain coupling leads to significant suppression of both plasmon oscillations as well as exciton formation in nanocomposites.<sup>10-12</sup>

Although the interplay between the excitons and plasmons has been much studied in quantum confined systems, apparently there is no report about such interactions in amorphous/glassy

<sup>a</sup>Author to whom correspondence should be addressed. Electronic mail: [adarsh@iiserb.ac.in](mailto:adarsh@iiserb.ac.in)

thin films. In general, it is a real challenge to observe directly the exciton-plasmon coupling in amorphous materials since the excitons are self-trapped at fast time scales, owing to the structural flexibility associated with the amorphous network.<sup>13,14</sup> Unlike crystalline semiconductors, usually these materials do not show any exciton fluorescence since they have many defect states and have indirect bandgap.<sup>15,16</sup> As a result, we have an outstanding problem connecting the optical nonlinearity of excitons, which defines their photosensitivity, with the field enhancement shown by the plasmons. In this letter, we demonstrate plasmon-exciton interaction at the ultrafast time scale in an amorphous Ge<sub>24</sub>Se<sub>76</sub>/gold nanoparticle (AuNP) heterostructure, which can be controlled by varying the plasmon wavelength. Our studies show that the coupling in these heterostructures is strong enough such that the exciton and plasmon absorptions are dramatically quenched. Further, the magnitude of quenching is strongly correlated with the plasmon wavelength.

Strongly coupled exciton-plasmon heterostructures of a-Ge<sub>24</sub>Se<sub>76</sub>/AuNP were prepared by sequential thermal evaporation and a step-by-step process is outlined in Fig. 1(a). To prepare the AuNP, we deposited a 15 nm thin gold layer on a quartz substrate. Half of the substrate was masked such that gold was coated only in region R1. The AuNP was formed by Ostwald ripening when the film was annealed at 550 °C for nearly 2 h in air.<sup>17,18</sup> Atomic force microscope (AFM) images of the AuNP in Fig. 1(a) show that the average particle size was 60 nm. The plasmon resonance was varied by controlling the annealing temperature (350 °C–550 °C) and thus manipulating the size of nanoparticles. To facilitate a strong coupling between the exciton and the localized surface plasmon, we deposited a-Ge<sub>24</sub>Se<sub>76</sub> thin film of 450 nm thickness over the AuNP by thermal evaporation. The coating was carried out after removing the mask such that we have regions of a-Ge<sub>24</sub>Se<sub>76</sub> and a-Ge<sub>24</sub>Se<sub>76</sub>/AuNP on the same substrate. Region R2 in Fig. 1(a) shows the bare a-Ge<sub>24</sub>Se<sub>76</sub> and R3 shows the heterostructure. AFM analysis showed that the surface roughness of the pure chalcogenide layer was less than 1 nm, but nearly 5 nm for the a-Ge<sub>24</sub>Se<sub>76</sub>/AuNP heterostructure.

To evaluate the plasmonic properties, we recorded the optical transmission spectrum of the AuNP as shown in Fig. 1(b). The surface plasmon resonance (SPR) of our AuNP is established by a dip in the transmission spectrum. The transmission spectra of the AuNP layer with three different sizes (60, 80, and 100 nm) are shown in Fig. S1(a) of the [supplementary material](#). The SPR wavelength range is the key to understand the nature of the interaction between a-Ge<sub>24</sub>Se<sub>76</sub> and AuNP, such that the bandgap value of the former should match the SPR of the latter.<sup>19</sup> Using the

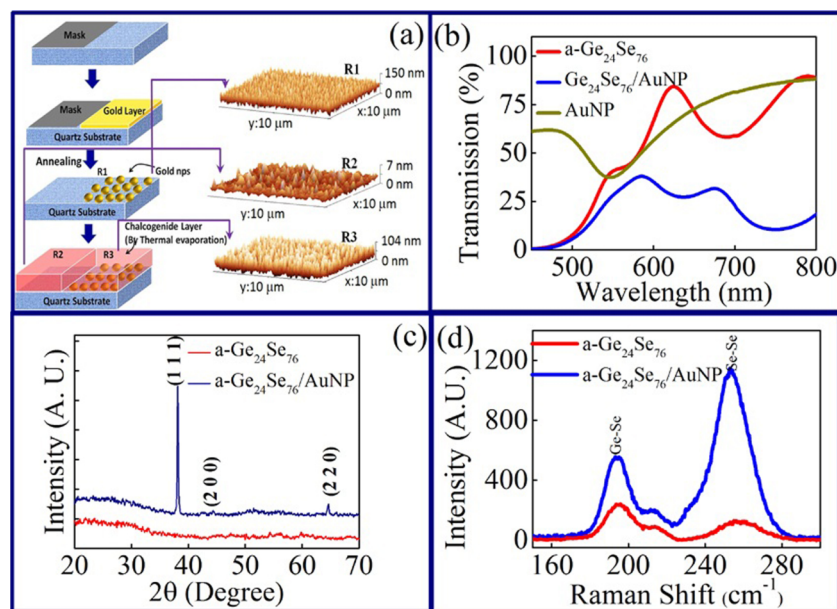


FIG. 1. (a) Schematic showing the method of preparation of the AuNP, a-Ge<sub>24</sub>Se<sub>76</sub> and their heterostructure. In the figure, R1, R2, and R3 are the topographic AFM images of the AuNP, a-Ge<sub>24</sub>Se<sub>76</sub> and heterostructure, respectively, (b) optical absorption (c) XRD, and (d) Raman spectra of a-Ge<sub>24</sub>Se<sub>76</sub> (red) and heterostructure (blue).

transmission spectrum of the a-Ge<sub>24</sub>Se<sub>76</sub> thin film shown in Fig. 1(b) (region R2 of the sample), we have calculated the optical bandgap as  $2.27 \pm 0.01$  eV ( $\sim 545$  nm) using Tauc plot (Fig. S2 of the supplementary material). At first, we selected the sample such that SPR of the AuNP at a wavelength of  $\sim 545$  nm matched with the optical bandgap of a-Ge<sub>24</sub>Se<sub>76</sub>. The transmission spectrum of the heterostructure shown in Fig. 1(b) is a combination of the individual spectrum of a-Ge<sub>24</sub>Se<sub>76</sub> and AuNP. The powder X-ray diffraction pattern of a-Ge<sub>24</sub>Se<sub>76</sub>/AuNP shown in Fig. 1(c), is simply a sum of the constituents, viz. AuNP and a-Ge<sub>24</sub>Se<sub>76</sub> layers. Here the crystalline nature of the AuNP is evidenced by characteristic (111), (200), and (220) reflections at  $2\theta = 38^\circ$ ,  $44^\circ$ , and  $64^\circ$  (JCPDS No-893697). Likewise, the broad featureless pattern observed alongside peaks from the AuNP confirms the amorphous nature of the Ge<sub>24</sub>Se<sub>76</sub> layer. The Raman spectra of as-prepared a-Ge<sub>24</sub>Se<sub>76</sub> and the heterostructure shown in Fig. 1(d) contain two vibrational modes, one from the corner sharing Ge-Se tetrahedra at  $193\text{ cm}^{-1}$  and the other from Se-Se polymeric chain at  $256\text{ cm}^{-1}$ .<sup>20</sup> Strikingly, there is a large enhancement of the intensity of Ge-Se and Se-Se Raman signals in the heterostructures, which can be attributed to the surface enhanced Raman scattering.<sup>21,22</sup>

To study the coupling between the exciton and the localized surface plasmon, we have employed femtosecond (fs) time resolved pump-probe transient absorption (TA) spectroscopy (for details see Ref. 23). Briefly, the pump is 120 fs pulse laser centered at 545 nm that excites the sample, and a time-delayed probe pulse measures the absorption change induced by the pump beam at the exciton-plasmon resonance. To evaluate the exciton-plasmon coupling, first, let us focus on the spectral and temporal evolution of TA spectra of the pure AuNP and a-Ge<sub>24</sub>Se<sub>76</sub> thin film. TA of the samples at various delay times in the wavelength range 560–850 nm of the probe beam following the pump beam excitation is mapped in the contour plots in Fig. 2. For better insight, several cross sections of the contour are shown in the right panels of the figure. The change in absorbance is calculated as  $\Delta A = -[\log(I_{\text{ex}}/I_0)]$ , where  $I_{\text{ex}}$  and  $I_0$  are the transmitted intensities of probe pulses

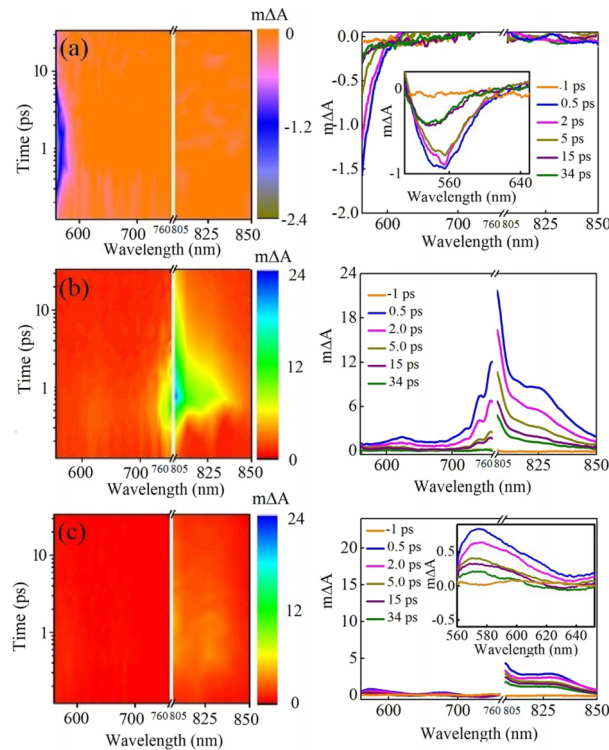


FIG. 2. Contour plots and cross sections of TA spectra of (a) AuNP (b) a-Ge<sub>24</sub>Se<sub>76</sub>, and (c) a-Ge<sub>24</sub>Se<sub>76</sub>/AuNP heterostructure at different probe delays. TA of the AuNP shows bleaching over a wavelength range overlapping with the SPR, while a-Ge<sub>24</sub>Se<sub>76</sub> shows strong TA in sub bandgap regions. Inset in (a) shows transient bleaching of the AuNP for 400 nm excitation. In the heterostructure, TA in the TD region (above 620 nm) and transient bleaching of the AuNP are completely suppressed. The inset in (c) shows TA in the bandgap region.

after a delay time  $\tau$  after excitation by the pump beam, and in the ground state, respectively. The  $\Delta A$  spectra of the AuNP in Fig. 2(a) show a pronounced bleaching over a wavelength range that overlaps with the SPR peak; the inset shows the data for the 400 nm pump pulse excitation (details in the [supplementary material](#)). The bleaching signal of the AuNP is attributed to the broadening of the SPR by the dephasing of the plasma oscillations, which causes a characteristic dip at the SPR.<sup>24,25</sup> The TA spectrum of a-Ge<sub>24</sub>Se<sub>76</sub> (Fig. 2(b)) spans from bandgap to sub-bandgap regions, with characteristic maxima occurring in the sub-bandgap region.<sup>26</sup> The strong TA in the sub-bandgap region is a direct evidence of the self-trapping of loosely bound Wannier-Mott (W-M) excitons that span across many atoms.<sup>15,27</sup> Since the formation energy of coordination defects is significantly lower than the W-M exciton and the bandgap energy, the W-M excitons are highly unstable. Subsequently, they interact with the lattice to form transient coordination defects (TDs), which exactly correspond to the self-trapping of excitons.<sup>15</sup> These TDs create states in the gap and generate more pronounced TA in the sub-bandgap region. Strikingly, the TA spectrum of the a-Ge<sub>24</sub>Se<sub>76</sub>/AuNP heterostructure (Fig. 2(c)) shows a dramatic suppression of the TA in the sub-bandgap region. The zoomed region in the inset of Fig. 2(c) shows that the AuNP plasmon bleaching is also suppressed. Thus, our fs TA measurements provide a direct evidence of the strong coupling of exciton and localized surface plasmon in the a-Ge<sub>24</sub>Se<sub>76</sub>/AuNP heterostructure.

To provide a consistent picture of quenching of TA in the a-Ge<sub>24</sub>Se<sub>76</sub>/AuNP heterostructure, we propose that the photoexcited electrons are temporarily transferred to the AuNP. This process results in the dissociation of excitons, which significantly reduces the self-trapping in a-Ge<sub>24</sub>Se<sub>76</sub> domains. As a result, we observe very weak TA in the sub-bandgap region. The validity of this assumption is supported by the fact that the AuNP bleaching signal is also suppressed. The pump beam induced transfer of the excited electrons from a-Ge<sub>24</sub>Se<sub>76</sub> to AuNP leaves the latter with an excessive negative charge, which removes the energy difference between the conduction states of both the layers.<sup>12</sup> Consequently, the electronic wave functions of both the regions overlap partly at the interface and result in the delocalization of plasma electrons. Such delocalization induced suppression of plasmon resonance was observed in Au/CdS nano-composites.<sup>12</sup> Indeed, the transfer of photo excited electrons from a-Ge<sub>24</sub>Se<sub>76</sub> to AuNP leads to the mixing of the electronic wave function and modified conduction states for both the layers, and serves as interfacial trap states.<sup>12</sup> We assume that the excited electrons occupying these states are uniformly distributed across the AuNP and a-Ge<sub>24</sub>Se<sub>76</sub> layers. Certainly, such an effect will result in the suppression of bleaching in the AuNP and sub-bandgap TA in a-Ge<sub>24</sub>Se<sub>76</sub>, as observed in our experiments.

The contribution of interfacial trap states can be determined from the decay kinetics of TA because the rate constants for all the three processes (plasmon bleach, self-trapping, and interfacial trap states) are indeed different. Figure 3(a) shows the temporal evolution of TA of the three samples. At these wavelengths, we used a bi-exponential function of the following form to fit the experimental data,<sup>26</sup>

$$\Delta A(t, \lambda) = i(t) \otimes \sum_1^2 A_l(\lambda) \exp(-t/\tau_l), \quad (1)$$

where  $i(t)$ ,  $A_l(\lambda)$ ,  $\tau_l$ , and  $\otimes$  are instrument response function, amplitude of the exponential decay, decay time constant (time for  $A_l(\lambda)$  to decay to 1/e of its original value), and the convolution operator, respectively. Fig. 3(a) shows the temporal profile of the plasmonic spectral region of the AuNP, which is fitted to two decay functions with relaxation times  $\tau_1 = 2.0 \pm 0.5$  ps and  $\tau_2 = 30 \pm 0.5$  ps. The fast decay constant represents the decay through electron–electron interaction and the slow component is attributed to decay through electron–phonon interactions.<sup>28</sup> The decay kinetics of a-Ge<sub>24</sub>Se<sub>76</sub> (Fig. 3(b)) also resulted in two time constants. The shorter value ( $\tau_1 = 1.4 \pm 0.4$  ps) corresponds to thermalization of the excitation driven hot carriers to the bottom of the conduction band (CB).<sup>26</sup> The slower decay process ( $\tau_2 = 29.4 \pm 0.2$  ps) involves the self-trapping of excitons in the mid-gap states of the chalcogenide matrix.<sup>15,26</sup>

The TA of the Ge<sub>24</sub>Se<sub>76</sub>/AuNP heterostructure can also be fitted to two exponentials with  $\tau_1 = 2.7 \pm 0.4$  ps and  $\tau_2 = 62 \pm 1$  ps. By comparing the  $\tau_1$  values of the Ge<sub>24</sub>Se<sub>76</sub>/AuNP heterostructure with Ge<sub>24</sub>Se<sub>76</sub> and AuNP, it can be seen that the thermalization time is not much

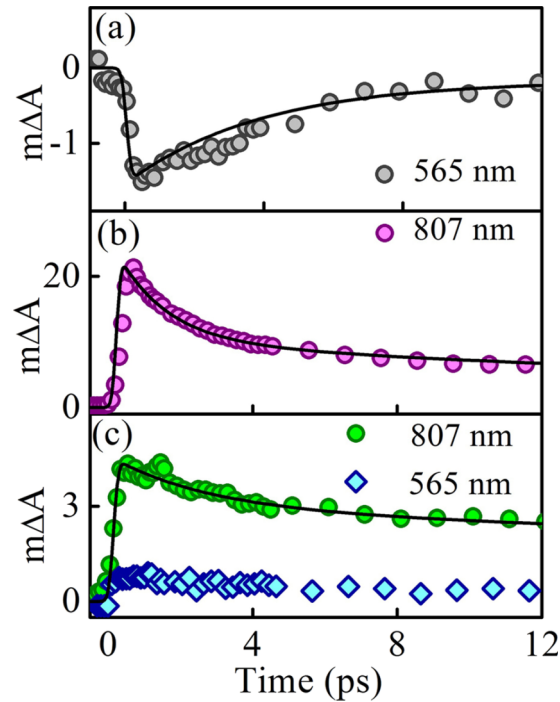


FIG. 3. Temporal evolution of TA corresponding to (a) plasmonic ( $\lambda = 565$  nm, grey circles) absorption of the isolated AuNP, (b) W-M exciton ( $\lambda = 807$  nm, pink circles) TA of a-Ge<sub>24</sub>Se<sub>76</sub>, and (c) the respective wavelengths in the heterostructure. The solid lines represent theoretical fits.

affected. However, the  $\tau_2$  values of a-Ge<sub>24</sub>Se<sub>76</sub> and AuNP are significantly shorter than that for the Ge<sub>24</sub>Se<sub>76</sub>/AuNP heterostructure (Fig. 3(c)). This clearly indicates that the decay of TA is significantly slower in the heterostructure, presumably originating from interfacial trap states formed by the strong exciton–plasmon coupling. In this regime, the excited carriers are trapped at the interfacial sites between the a-Ge<sub>24</sub>Se<sub>76</sub> and AuNP. However, since such sites are absent in a-Ge<sub>24</sub>Se<sub>76</sub> or AuNP, the excited carrier population decreases faster and results in short lived TA.

To get new insight into the dependence of SPR wavelength on the quenching of TA, we have prepared samples consisting of the AuNP with three plasmon wavelengths, made by varying the diameters of the nanoparticles shown in Fig. S1(a) of the [supplementary material](#). The position of the plasmon wavelength shifts to longer wavelengths with the increase in particle size. Hereafter we identify the a-Ge<sub>24</sub>Se<sub>76</sub>/AuNP heterostructures as HS1, HS2, and HS3, having the plasmon resonance wavelengths 545, 580, and 620 nm, respectively.

Fig. 4(a) shows the temporal evolution of the TA maxima at 807 nm of the three heterostructures. Notably, the magnitude of TA decreases greatly as the plasmon wavelength approaches the bandgap of a-Ge<sub>24</sub>Se<sub>76</sub>. Clearly, the quenching of TA of a-Ge<sub>24</sub>Se<sub>76</sub>/AuNP can be controlled by adjusting the SPR wavelength. The suppression of TA as a function of plasmon wavelength indicates that the charge separation from a-Ge<sub>24</sub>Se<sub>76</sub> to AuNP is directly affected by the size of the AuNP. Our experimental results clearly show that the delocalization of the plasma electrons is most effective when the AuNP SPR wavelength lies near the CB of the chalcogenide layer, as noted by Khon *et al.*<sup>12</sup> and Ben-Shahar *et al.*<sup>29</sup> Such delocalization is not prominent in HS2 and HS3 heterostructures since SPR is far away from the bandgap of a-Ge<sub>24</sub>Se<sub>76</sub>. We have fitted the decay of the TA of the three heterostructures at 807 nm by using Eq. (1) and the decay constants are shown in Table I. Note that their TA decay rates are significantly different since the interfacial charge transfer strongly depends on the position of the SPR band of the AuNP with respect to the bandgap of a-Ge<sub>24</sub>Se<sub>76</sub>. Photoexcited carriers in the chalcogenide layer can relax via electron transfer to the metal domain or by self-trapping of excitons.<sup>15</sup> As shown in Fig. 4(b), when the Au SPR matches the CB of a-Ge<sub>24</sub>Se<sub>76</sub>, the probability of inter-domain charge transfer is more than that

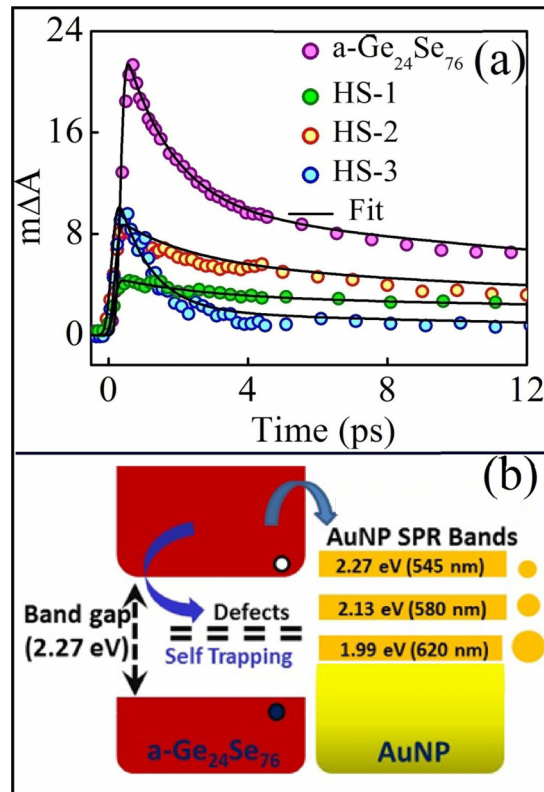


FIG. 4. (a) Temporal kinetics of TA for different heterostructures. (b) Schematic representing the quenching of exciton bands via interfacial charge transfer in the a-Ge<sub>24</sub>Se<sub>76</sub>/AuNP heterostructure. Magnitude of quenching depends on the position of the Au SPR band which in turn depends on the size of the AuNP.

for self-trapping.<sup>30</sup> Therefore, the decay rates of HS1 are slower than those for pure a-Ge<sub>24</sub>Se<sub>76</sub> and other two heterostructures. As the size of the AuNP increases, the difference between the Au SPR band and chalcogenide CB increases. Due to this variation, the barrier at the interface is high, and the probability of self-trapping overcomes the electron transfer to the AuNP. Once the excitons are trapped in the chalcogenide defect states, the electrons are localized, obstructing the charge transfer to the AuNP. This assumption is supported by the fact that the decay rates of HS2 and HS3 are comparable to those of a-Ge<sub>24</sub>Se<sub>76</sub>.

In conclusion, we have demonstrated that the plasmon-exciton interaction at the ultrafast time scale in an amorphous Ge<sub>24</sub>Se<sub>76</sub>/AuNP heterostructure can be controlled by varying the plasmon wavelength. Our studies show that the strong coupling in these heterostructures leads to dramatic suppression of exciton and plasmon absorptions. Further, exciton quenching is found to be most efficient when the SPR wavelength matches the optical bandgap, which can be readily controlled by adjusting the plasmon wavelength that depends on the size of the AuNP. The results are explained by assuming the transfer of photo excited electrons from a-Ge<sub>24</sub>Se<sub>76</sub> to AuNP, which then leads to the mixing of the electronic wave function and the formation of interfacial trap states. Thus we

TABLE I. Decay time constants and amplitudes of the interfacial trap states obtained from the bi-exponential fit.

Sample	mΔA	$\tau_1$ (ps)	$\tau_2$ (ps)
HS1	4.4 ( $\pm 0.2$ )	2.7 ( $\pm 0.4$ )	62 ( $\pm 1$ )
HS2	8.4 ( $\pm 0.5$ )	2.2 ( $\pm 0.2$ )	33 ( $\pm 2$ )
HS3	9.6 ( $\pm 0.5$ )	0.90 ( $\pm 0.06$ )	17 ( $\pm 2$ )

envision that exciton-plasmon coupling in amorphous material and metallic hybrid structures offers far-reaching opportunities for new optical functionalities for the development of novel device technologies, for example, optical data storage, surface enhanced Raman scattering, and semiconductor devices.

See [supplementary material](#) for the optical absorption spectrum of the AuNP, Tauc bandgap calculation of a-Ge<sub>24</sub>Se<sub>76</sub> thin film, and transient absorption spectrum of all samples at 400 nm excitation.

The authors thank Department of Science and Technology (Project No. SR/S2/LOP-003/2010) and Council of Scientific and Industrial Research, India (Grant No. 03(1250)/12/EMR-II) for financial support. The work in Hungary is supported by the TÁMOP-4.2.2. A-11/1/KONV-2012-0036 project, and co-financed by the European Union and the European Social Fund. The US National Science Foundation is gratefully acknowledged for supporting international collaboration through International Materials Institute for New Functionality in Glass (Grand No. DMR-0844014).

- <sup>1</sup> S. M. Sadeghi, A. Hatef, and M. Meunier, *Appl. Phys. Lett.* **102**, 203113 (2013).
- <sup>2</sup> Y. Zhao, S. Li, Y. Zeng, and Y. Jiang, *APL Mater.* **3**, 86103 (2015).
- <sup>3</sup> C. Gonzalez-Ballester, J. Feist, E. Moreno, and F. J. Garcia-Vidal, *Phys. Rev. B* **92**, 121402 (2015).
- <sup>4</sup> C. Li, X. Li, L. Cao, G. Jin, and M. Gu, *Appl. Phys. Lett.* **102**, 251115 (2013).
- <sup>5</sup> K.-D. Kim, T. Pfadler, E. Zimmermann, Y. Feng, J. A. Dorman, J. Weickert, and L. Schmidt-Mende, *APL Mater.* **3**, 106105 (2015).
- <sup>6</sup> N. T. Fofang, T.-H. Park, O. Neumann, N. A. Mirin, P. Nordlander, and N. J. Halas, *Nano Lett.* **8**, 3481 (2008).
- <sup>7</sup> K. T. Shimizu, W. K. Woo, B. R. Fisher, H. J. Eisler, and M. G. Bawendi, *Phys. Rev. Lett.* **89**, 117401 (2002).
- <sup>8</sup> P. Vasa, W. Wang, R. Pomraenke, M. Lammers, M. Maiuri, C. Manzoni, G. Cerullo, and C. Lienau, *Nat. Photonics* **7**, 128 (2013).
- <sup>9</sup> D. G. Lidzey, D. D. C. Bradley, M. S. Skolnick, T. Virgili, S. Walker, and D. M. Whittaker, *Nature* **395**, 53 (1998).
- <sup>10</sup> J. Bellessa, C. Bonnand, J. C. Plenat, and J. Mugnier, *Phys. Rev. Lett.* **93**, 36404 (2004).
- <sup>11</sup> R. Sharma, J. Aneesh, R. K. Yadav, S. Sanda, A. R. Barik, A. K. Mishra, T. K. Maji, D. Karmakar, and K. V. Adarsh, *Phys. Rev. B* **93**, 155433 (2016).
- <sup>12</sup> E. Khon, A. Mereshchenko, A. N. Tarnovsky, K. Acharya, A. Klinkova, N. N. Hewa-Kasakarage, I. Nemitz, and M. Zamkov, *Nano Lett.* **11**, 1792 (2011).
- <sup>13</sup> R. Sharma, D. Kumar, V. Srinivasan, H. Jain, and K. V. Adarsh, *Opt. Express* **23**, 14085 (2015).
- <sup>14</sup> B. J. Eggleton, B. Luther-Davies, and K. Richardson, *Nat. Photon.* **5**, 141 (2011).
- <sup>15</sup> D. K. Biegelsen and R. A. Street, *Phys. Rev. Lett.* **44**, 803 (1980).
- <sup>16</sup> J. Berashevich, A. Mishchenko, and A. Reznik, *Phys. Rev. Appl.* **1**, 34008 (2014).
- <sup>17</sup> M. J. Rost, D. A. Quist, and J. W. M. Frenken, *Phys. Rev. Lett.* **91**, 026101 (2003).
- <sup>18</sup> S. Charnovych, I. A. Szabó, A. L. Tóth, J. Volk, M. L. Trunov, and S. Kökényesi, *J. Non-Cryst. Solids* **377**, 200 (2013).
- <sup>19</sup> R. Jiang, B. Li, C. Fang, and J. Wang, *Adv. Mater.* **26**, 5274 (2014).
- <sup>20</sup> P. Khan, H. Jain, and K. V. Adarsh, *Sci. Rep.* **4**, 4029 (2014).
- <sup>21</sup> A. Campion and P. Kambhampati, *Chem. Soc. Rev.* **27**, 241 (1998).
- <sup>22</sup> P. Alonso-González, P. Albella, M. Schnell, J. Chen, F. Huth, A. García-Etxarri, F. Casanova, F. Golmar, L. Arzubia, L. E. Hueso, J. Aizpurua, and R. Hillenbrand, *Nat. Commun.* **3**, 684 (2012).
- <sup>23</sup> R. Sharma, K. Prasai, D. A. Drabold, and K. V. Adarsh, *AIP Adv.* **5**, 77164 (2015).
- <sup>24</sup> R. Sundararaman, P. Narang, A. S. Jermyn, W. A. Goddard III, and H. A. Atwater, *Nat. Commun.* **5**, 5788 (2014).
- <sup>25</sup> S. Link, C. Burda, M. B. Mohamed, B. Nikoobakht, and M. A. El-Sayed, *Phys. Rev. B* **61**, 6086 (2000).
- <sup>26</sup> A. R. Barik, M. Bapna, D. A. Drabold, and K. V. Adarsh, *Sci. Rep.* **4**, 3686 (2014).
- <sup>27</sup> P. Khan, T. Saxena, and K. V. Adarsh, *Opt. Lett.* **40**, 768 (2015).
- <sup>28</sup> T. S. Ahmadi, S. L. Logunov, and M. A. El-Sayed, *J. Phys. Chem.* **100**, 8053 (1996).
- <sup>29</sup> Y. Ben-Shahar, F. Scotognella, I. Kriegel, L. Moretti, G. Cerullo, E. Rabani, and U. Banin, *Nat. Commun.* **7**, 10413 (2016).
- <sup>30</sup> J. Dana, T. Debnath, P. Maity, and H. N. Ghosh, *J. Phys. Chem. C* **119**, 22181 (2015).